Total cross sections for production of ^{7}Be, ^{22}Na, and ^{24}Na in $p+^{7}$Li and $p+^{27}$Al reactions at 495 and 795 MeV

T. N. Taddeucci, J. Ullmann, L. J. Rybarcyk, and G. W. Butler
Los Alamos National Laboratory, Los Alamos, New Mexico 87545

T. E. Ward
U.S. Department of Energy, Washington, D.C. 20585

(Received 11 September 1996; revised manuscript received 19 November 1996)

Activation techniques have been used to measure the total cross section for the production of ^{7}Be, ^{22}Na, and ^{24}Na in proton induced reactions on ^{7}Li and ^{27}Al targets at bombarding energies of 495 MeV and 795 MeV. The cross section for the ^{7}Li$(p,n)^{7}$Be(g.s.+0.43-MeV) reaction at 795 MeV is about 11–15 % larger than extrapolations based on previous data below 480 MeV. [S0556-2813(97)03403-1]

PACS number(s): 25.40.Ep, 25.40.Sc

The ^{7}Li(p,n) reaction leading to the ground state and first excited state (0.43 MeV) in ^{7}Be is a convenient reaction to employ for normalization purposes. Because there are no particle-emission stable states above the first excited state, the total cross section for this reaction can be measured by counting residual ^{7}Be nuclei. The total cross section can also be obtained, to within an overall normalization factor, by integrating the differential-cross-section angular distribution for the (g.s. + 0.43-MeV) transition. Comparison of the two results gives the proper normalization factor for the differential-cross-section distribution [1].

Differential-cross-section distributions have been measured for energies up to 795 MeV [2]. Until the present experiment, however, total cross sections obtained from activation measurements existed only for energies up to 480 MeV [3]. Normalization of higher-energy differential cross sections has therefore been dependent upon an extrapolation of the activation total cross sections for energies above 480 MeV [2]. We report here new ^{7}Li$(p,n)^{7}$Be activation measurements that extend the range of the total cross section data up to 795 MeV. Aluminum targets were also irradiated under the same conditions as the lithium targets to provide a check on the normalization of the data. The cross sections for production of ^{7}Be, ^{22}Na, and ^{24}Na in the aluminum are also reported.

The experiment was performed at the Clinton P. Anderson Meson Physics Facility (LAMPF) in Los Alamos. Targets were irradiated in the target chamber of the Neutron Time-of-flight (NTOF) facility. The beam current was monitored by scaling the output from a secondary emission monitor (designated NTER1) 10 m upstream from the target, and by integrating the charge collected in an insulated graphite beam stop (NTFC) 7 m downstream from the target. NTER1 was continuously in the beam during all irradiations. The normalization of the NTER1 and NTFC currents was checked by comparison to a calibrated toroid (LXCM3) in an upstream beam stop. This comparison revealed a small intensity dependence (nonlinearity) to both the NTER1 and NTFC outputs. Over a range of beam currents from 30 nA to 250 nA, the NTER1 output decreased by 3.3%. Over the same range, the NTFC output increased by 4.1%. Correction for this intensity dependence has been made in the analysis of the data. Beam intensity for the 495-MeV irradiations was in the range from 27 to 32 nA. Beam intensity for the 795-MeV irradiations was in the range from 50 to 200 nA.

Three target assemblies were irradiated at each beam energy. The first assembly consisted of three layers of rolled lithium metal (99.9% ^{7}Li, 1 mm, 2.7 mm, and 1 mm thick) followed downstream by three aluminum plates (1100-H14 alloy, $>$99% Al, each 1.63 mm thick). The second assembly consisted of a single layer of rolled lithium metal (96.5% ^{7}Li, 2 mm thick). The third assembly consisted of three aluminum plates (each 1.63 mm thick). The areal dimensions of each target piece were 3.8 cm $\times$ 4.8 cm. The beam spot size was about 2.5 cm (full width) at 495 MeV and about 1.0 cm (full width) at 795 MeV. Beam positioning was guided by insertable wire scanners approximately 30 cm upstream and downstream from the target position, and by a phosphor on the target ladder. The beam was centered to an accuracy of better than 1 mm.

The thickness of the aluminum plates in the three-layer stacks was chosen to be sufficiently large to stop high-energy ^{7}Be fragments. In the middle target, forward and backward losses are therefore compensated by gains from the upstream and downstream targets. Detailed measurements of ^{7}Be production for protons incident on silver at 480 MeV [4] showed a peak fragment energy of about 30 MeV. At backward angles, contributions from fragments as high as 100 MeV are down by 5 orders of magnitude. The energy distribution for ^{7}Be fragments from aluminum peaks at lower energies (e.g., see [5]), therefore use of the silver distributions provides a conservative estimate of the necessary target thickness. The aluminum targets used here will stop 191-MeV ^{7}Be fragments.

Target thickness (areal density) was determined by dividing the measured mass by the measured area. Target mass was determined by weighing each piece (as well as standard reference masses) with both an electronic balance and a triple-beam balance. Results from the two balances agreed at the 0.5% level. Uniformity of target thickness was checked with a micrometer by measuring at the center of each target and at several points around the edge. Each target was uni-

TABLE I. Total cross sections (mb) for proton induced reactions on aluminum. The error bars represent an overall systematic uncertainty of 3.5%.

Reaction	495 MeV	795 MeV
^{27}Al$(p,x)^{7}$Be	3.6±0.1	5.3±0.2
^{27}Al$(p,3p3n)^{22}$Na	14.3±0.5	13.2±0.5
^{27}Al$(p,3pn)^{24}$Na	10.3±0.4	10.6±0.4

form to within the resolution of the micrometer (0.025 mm). Measured target densities agree with standard reference values to better than 1%.

Isotopic purity and surface contamination of the lithium targets was checked by examining time-of-flight (TOF) spectra obtained during each irradiation. The standard NTOF detector array [2], positioned at a flight path of 170 m, was used for these measurements. The TOF spectra revealed no detectable contributions from (p,n) reactions on ^{12}C, ^{14}N, or ^{16}O (the most likely contaminants after storage in mineral oil and exposure to air). Furthermore, the relative intensity of the ^{6}Li(p,n) and ^{7}Li(p,n) peaks observed in the single-layer lithium data is consistent with the assay isotopic fraction to better than 1%. No ^{6}Li contribution was observed in the data from the stacked lithium targets.

The number of ^{7}Be atoms produced in the irradiations was determined by counting the 478-keV gamma rays following the (10.45±0.04)% [6] electron-capture decay branch of ^{7}Be. The aluminum targets were also monitored for 1369-keV gamma rays from the decay of ^{24}Na produced by the ^{27}Al$(p,3pn)^{24}$Na reaction, and for 1274-keV gamma rays from the decay of ^{22}Na produced by the ^{27}Al$(p,3p3n)^{22}$Na reaction. All targets were counted in a set of standard geometries with HPGe detectors. The HPGe detector efficiencies were determined from calibrated reference sources and were corrected for target thickness and spot size. Each target was counted between four and eight times over a period of about ten days. Statistical uncertainties in the resultant gamma-ray activities are $<0.5\%$ for the aluminum targets and $<1.5\%$ for the lithium targets.

Aluminum cross sections are obtained from an unweighted average of the results for the two middle targets at each energy. An unweighted average is used because relative systematic uncertainties (target thickness, beam integration) are larger than the statistical uncertainties. The aluminum results are presented in Table I and are plotted with a selection of previous measurements [7–14] in Fig. 1.

Values for the ^{7}Li$(p,n)^{7}$Be cross section are obtained from the upstream (U) and single (S) targets only, to avoid corrections for backward contamination from aluminum. Such contamination is evident in the data from the downstream targets (adjacent to the three-layer aluminum stack), where normalized ^{7}Be yields at 495 MeV and 795 MeV are 13% and 22% larger, respectively, than the yields from the upstream targets. This enhancement is consistent with Monte Carlo estimates based on the energy and angle distributions for ^{7}Be fragment production in silver [4]. Results from the middle and upstream lithium targets differ by less than 2% at each energy, but we rule out use of the middle-target data as well because of similar concerns about contamination (estimated to be $<3\%$).

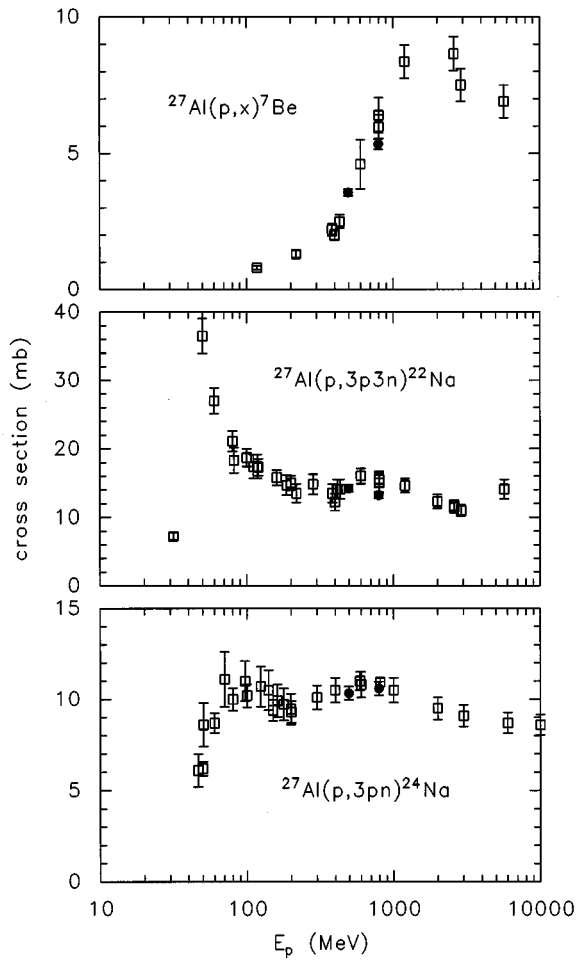

FIG. 1. Total cross sections for production of ^{7}Be (top), ^{22}Na (middle), and ^{24}Na (bottom). Results from the present experiment are represented as solid circles. The open boxes represent a selection of previous measurements [7–14].

The ^{7}Li$(p,n)^{7}$Be results are presented in Table II, where the error bars represent an estimated 3.5% systematic uncertainty. The known primary contributions to this systematic uncertainty are target thickness (1%), beam integration (3%), and gamma-detector efficiency (1.5%). Results from the 18 targets in the three-layer stacks are internally consistent to better than 2.5% (maximum deviation from the mean for each transition). Results from the aluminum targets all agree

TABLE II. Total cross sections (mb) for the ^{7}Li$(p,n)^{7}$Be(g.s.+0.43-MeV) reaction. The first two lines correspond to results from the upstream (U) and single (S) targets. The next two lines are extrapolations based on previous data ($E_p<480$ MeV): σ_T(log) is from power-law fit I in Table III, $\sigma_T(I_q)$ is the constant-I_q fit from Ref. [2]. The last line is the ratio (sr^{-1}) of 0° lab cross section to total cross section from Ref. [2].

	495 MeV	795 MeV
$\sigma_T(U)$	1.06±0.04	0.72±0.02
$\sigma_T(S)$	0.97±0.03	0.66±0.02
σ_T(log)	1.03±0.03	0.60±0.02
$\sigma_T(I_q)$	1.05±0.02	0.62±0.01
$\sigma_{\rm lab}(0°)/\sigma_T$	38.5±1.1	68.9±2.0

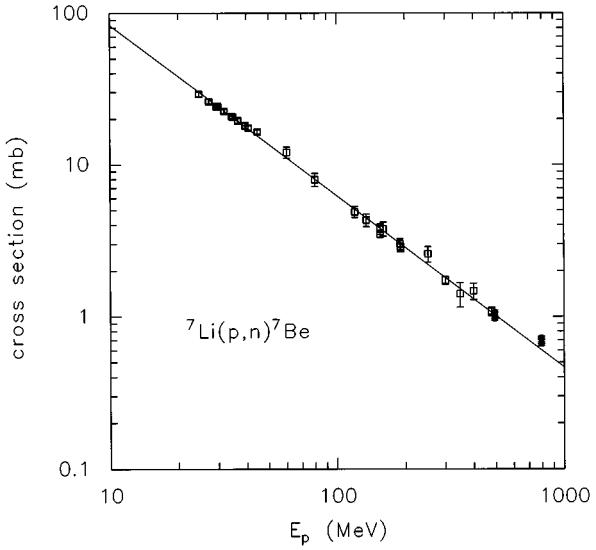

FIG. 2. Total cross section for the $^{7}\mathrm{Li}(p,n)^{7}\mathrm{Be}$(g.s.+0.43-MeV) reaction as a function of bombarding energy. The solid line corresponds to power-law fit I in Table III.

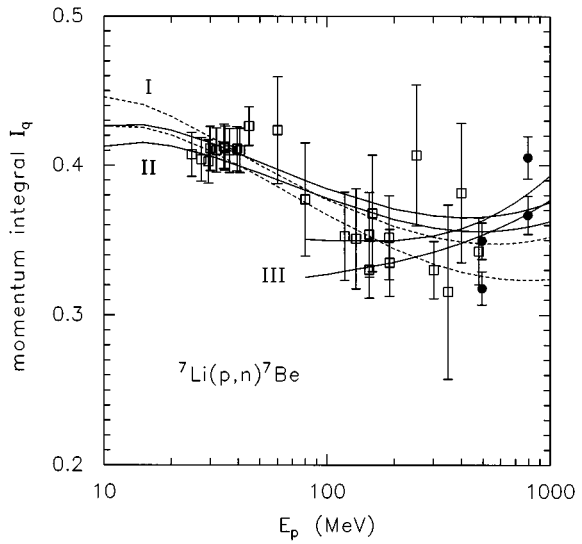

FIG. 3. The momentum-transfer integral I_q extracted from activation total cross sections. The labeled lines correspond to one-sigma error bands for fits I–III in Table III. The new data points are represented as solid circles, previous data are open boxes.

at this level before making recoil corrections. Similar consistency is observed for the stacked lithium targets, after estimating corrections for backscatter contamination in the downstream targets. Unfortunately, cross sections obtained from the two single lithium targets are about 10% lower than the values obtained from the stacked targets. While this strongly suggests an unrecognized systematic error of some sort, we can find no basis to reject these data. We present these results separately, however, because of this anomaly. Note that the lithium targets from the three-layer stacks share a common beam normalization factor with the aluminum targets. The $^{27}\mathrm{Al}(p,3pn)^{24}\mathrm{Na}$ cross section derived from these targets agrees with the independent measurement of Cumming, Agoritsas, and Witkover (10.94 ± 0.24 mb at 0.81 GeV) [7] to within 3%.

Figure 2 shows the new $^{7}\mathrm{Li}$ activation cross sections plotted with previous lower-energy data [1,3,15,16]. The solid line in this figure represents a power-law fit of the form

$$\sigma_{\mathrm{tot}}=e^{a}E_{p}^{b}, \tag{1}$$

with parameters obtained from *previous* data (25–480 MeV) [3]. The total cross section can also be written in a form that makes explicit the main source of energy dependence:

$$\sigma_{\mathrm{tot}}=\frac{2\pi}{k_i k_f}I_q, \tag{2}$$

where k_i and k_f are the initial and final wave numbers in the center-of-mass frame and I_q is the dimensionless integral of the differential cross section distribution over the allowed range of momentum transfer [2,16]. Values for the momentum integral I_q are plotted in Fig. 3. It was previously noted [2] that in the energy range from 80 to 480 MeV the data are consistent with a constant value $I_q=0.345\pm0.008$. It is clear from Fig. 3 that over the wider energy range from 25 to 795 MeV, this integral is not constant. The energy dependence of this quantity should reflect changes in the strength of the effective interaction and distortion effects [16].

The new total cross-section data are in good agreement with previous measurements near 500 MeV, but at 795 MeV are clearly larger than extrapolations from the old data. The average of the new data points at 795 MeV is about 11% larger than the constant-I_q extrapolation and about 15% larger than the previous power-law fit. Three power-law fits are presented in Fig. 3, where the lines represent one-sigma error bands for each fit. The dashed lines (fit I) spanning the width of the graph represent the fit to previous data only (25–480 MeV). The solid lines (fit II) spanning the width of the graph represent a fit that includes the new data reported here (25–800 MeV). This fit overestimates the cross section in the 100–500 MeV region. The solid lines (fit III) between 80 and 1000 MeV represent a limited-energy fit including the new data. This fit better represents the trend of the data above 100 MeV. Parameters of these fits are listed in Table III. The two fits that include the new data (II and III) yield estimated values at 795 MeV that are 8–11 % higher than the previous extrapolation (fit I).

The larger cross section at 795 MeV will force a readjustment of experimental normalizations only if the increase is due solely to (p,n) reaction strength. One other potential contributor to this increase could be alternate reaction channels such as $^{7}\mathrm{Li}(p,p'\pi^{-})^{7}\mathrm{Be}$ or $^{7}\mathrm{Li}(p,n\pi^{0})^{7}\mathrm{Be}$, which have been assumed to contribute negligibly because of the

TABLE III. Parameters for power-law fits to the $^{7}\mathrm{Li}(p,n)^{7}\mathrm{Be}$ total cross section $\sigma_{\mathrm{tot}}=e^{a}E_{p}^{b}$.

Fit	Energy range (MeV)	a	b
I	25–480	7.021 ± 0.051	-1.127 ± 0.013
II	25–795	6.919 ± 0.030	-1.100 ± 0.006
III	80–795	6.477 ± 0.123	-1.030 ± 0.020

large momentum transfer involved. However, the cross sections for free $np \rightarrow pp'\pi^-$ and $np \rightarrow pn\pi^0$ are about 2 mb and 6.5 mb, respectively, at 800 MeV [17]. These free cross sections are up to an order of magnitude larger than the ^{7}Li(p,n) total cross section, so even with large momentum-transfer inhibition, substantial contributions to ^{7}Be production may still occur. The $(p,p\pi^-)$ and $(p,n\pi^0)$ pion-production channels are isospin analogs of the $(p,n\pi^+)$ coherent-pion-production (CPP) mechanism described by Udagawa *et al.* [18]. A crude estimate based on their calculations of CPP for ^{12}C$(p,n\pi^+)$ appears to be consistent with the increase (80 ± 30 μb) observed here. Clearly, a realistic calculation is required to settle this important point. Alternately, an independent normalization of the 0° cross section would yield an unambiguous measure of the CPP cross section. If contributions from pion production prove to be significant, then normalization strategies that employ ^{7}Li(p,n) for energies far above pion threshold will have to be reconsidered.

This work was supported by the U.S. Department of Energy.

[1] S. D. Schery, L. E. Young, R. R. Doering, Sam M. Austin, and R. K. Bhowmik, Nucl. Instrum. Methods **147**, 399 (1977).
[2] T. N. Taddeucci, W. P. Alford, M. Barlett, R. C. Byrd, T. A. Carey, D. E. Ciskowski, C. C. Foster, C. Gaarde, C. D. Goodman, C. A. Goulding, E. Gülmez, W. Huang, D. J. Horen, J. Larsen, D. Marchlenski, J. B. McClelland, D. Prout, J. Rapaport, L. J. Rybarcyk, W. C. Sailor, E. Sugarbaker, and C. A. Whitten, Jr., Phys. Rev. C **41**, 2548 (1990).
[3] J. D-Auria, M. Dombsky, L. Moritz, T. Ruth, G. Sheffer, T. E. Ward, C. C. Foster, J. W. Watson, B. D. Anderson, and J. Rapaport, Phys. Rev. C **30**, 1999 (1984).
[4] Ray E. L. Green, Ralph G. Korteling, and K. Peter Jackson, Phys. Rev. C **29**, 1806 (1984).
[5] G. D. Westfall, R. G. Sextro, A. M. Poskanzer, A. M. Zebelman, G. W. Butler, and E. K. Hyde, Phys. Rev. C **17**, 1368 (1978).
[6] F. Ajzenberg-Selove, Nucl. Phys. **A490**, 66 (1988).
[7] J. B. Cumming, V. Agoritsas, and R. Witkover, Nucl. Instrum. Methods **180**, 37 (1981).
[8] J. B. Cumming, Annu. Rev. Nucl. Sci. **13**, 261 (1963).
[9] J. B. Cumming, J. Hudis, A. M. Poskanzer, and S. Kaufman, Phys. Rev. **128**, 2392 (1962).
[10] B. Dittrich, U. Herpers, M. Lüpke, R. Michel, H. J. Hofmann, and W. Wölfli, Radiochim. Acta **50**, 11 (1990).
[11] J. Tobailem and C. H. de Lassus St. Genies, Centre d'Etudes Nucleaires de Saclay, Report No. CEA-N-1466(5), 1981.
[12] H. R. Heydegger, Anthony L. Turkevich, A. Van Ginneken, and P. H. Walpole, Phys. Rev. C **14**, 1506 (1976).
[13] G. M. Raisbeck and F. Yiou, Phys. Rev. C **9**, 1385 (1974).
[14] R. Michel, F. Peiffer, and R. Stück, Nucl. Phys. **A441**, 617 (1985).
[15] L. Valentin, G. Albouy, J. P. Cohen, and M. Gusakow, Phys. Rev. Lett. **7**, 163 (1963); Nucl. Phys. **62**, 81 (1965).
[16] T. E. Ward, C. C. Foster, G. E. Walker, J. Rapaport, and C. A. Goulding, Phys. Rev. C **25**, 762 (1982).
[17] B. J. VerWest and R. A. Arndt, Phys. Rev. C **25**, 1979 (1982).
[18] T. Udagawa, P. Oltmanns, F. Osterfeld, and S. W. Hong, Phys. Rev. C **49**, 3162 (1994).